Andreev reflection in graphene nanoribbons

Diego Rainis,[1,*] Fabio Taddei,[1] Fabrizio Dolcini,[1] Marco Polini,[1] and Rosario Fazio[1,2]
[1]*NEST-CNR-INFM and Scuola Normale Superiore, I-56126 Pisa, Italy*
[2]*International School for Advanced Studies (SISSA), via Beirut 2-4, I-34014 Trieste, Italy*
(Received 18 November 2008; revised manuscript received 30 January 2009; published 27 March 2009)

We study Andreev reflection in graphene nanoribbon/superconductor hybrid junctions. By using a tight-binding approach and the scattering formalism we show that finite-size effects lead to notable differences with respect to the bulk-graphene case. At subgap voltages, conservation of pseudoparity, a quantum number characterizing the ribbon states, yields either a suppression of Andreev reflection when the ribbon has an even number of sites in the transverse direction or perfect Andreev reflection when the ribbon has an odd number of sites. In the former case the suppression of Andreev reflection induces an insulating behavior even when the junction is biased; electron conduction can however be restored by applying a gate voltage. Finally, we check that these findings remain valid also in the case of nonideal nanoribbons in which the number of transverse sites varies along the transport direction.

DOI: 10.1103/PhysRevB.79.115131 PACS number(s): 72.10.−d, 74.45.+c, 73.23.−b

I. INTRODUCTION

Graphene, a flat monolayer of carbon atoms arranged in a two-dimensional (2D) honeycomb lattice, is a newly realized 2D electron system[1] which has attracted a great deal of interest because of the novel physics which it exhibits and because of its potential as a new material for electronic technology. One of the fascinating aspects of this system is that in most cases its potentialities for device applications are intimately related with fundamental aspects of quantum mechanics. Many of the transport properties of graphene which are at the heart of the design of new functional nanostructures originate from conservation laws of certain quantum numbers. For example, the fact that electrostatic barriers in graphene are perfectly transparent to electron scattering with angles close to normal incidence (Klein paradox) is explained[2] in terms of the conservation of pseudospin (the sublattice degree of freedom necessary to describe graphene's non-Bravais honeycomb lattice[1]).

Early investigations on transport properties of graphene have analyzed current and noise in the presence of normal leads. Recent studies[3–9] have pointed out that novel interesting phenomena arise when graphene is interfaced to a superconductor (SC). In the seminal papers by Beenakker and co-workers[3] it was shown that the peculiar band structure of graphene gives rise to the appearance of specular Andreev reflection (AR),[10] a novel type of AR that is absent in ordinary metal/SC interfaces. These studies paved the way to experimental investigations of the proximity effect[11,12] and of supercurrent flow[13,14] in graphene. On the theoretical side the results of Ref. 3 have been extended in a number of ways, e.g., to graphene bilayers[4] and to the case of interfaces with *d*-wave SCs,[5] whereas further studies have focused on the subgap structure of SC-graphene-SC junctions,[6] on crossed AR,[7] and on magnetotransport.[8]

Most of the theoretical analyses carried out so far describe the graphene sheet as an infinite (or semi-infinite) 2D plane and identify two energy scales relevant for transport, namely, the superconducting gap Δ_0 and the potential difference between the normal side and the superconducting side, which allows, for instance, to switch from the regime of ordinary AR to the one of specular AR. In graphene ribbons,[15] however, the finite size of the sample yields an additional energy scale, δ, characterizing the mean energy spacing between the ribbon bands. Since the typical ribbon size varies from 10 nm up to 1 μm,[15] δ can range from 300 meV down to 3 meV, and it is thus larger than (or of the same order of) the typical superconducting gap $\Delta_0 \lesssim 1$ meV. As a consequence, δ is expected to play an important role in electron transport and AR in graphene.

In the present work we address this problem by analyzing electronic transport through a hybrid junction between a graphene nanoribbon (GNR) (Refs. 16–19) and a SC, as sketched in Fig. 1. We consider the case of a GNR with zigzag edges, which has been shown to represent fairly well the behavior of an arbitrarily shaped edge.[20]

Remarkable effects emerge due to the finite size of the GNR. We find that AR is strongly affected by the conservation of *pseudoparity*, a quantum number characterizing the GNR eigenstates, which depends on whether the number N_W of sites along the transverse direction is even or odd. In particular, while in GNRs with odd N_W the AR coefficient is unity for subgap voltages, in GNRs with an even N_W AR is totally suppressed. In the latter case AR can be restored to a finite value by applying a gate voltage. Even-odd effects with the same physical origin have been also found in normal transport through graphene *p-n* junctions (valley-valve effect).[21–23]

This paper is organized as follows. In Sec. II we introduce the tight-binding Hamiltonian that we use to model the GNR

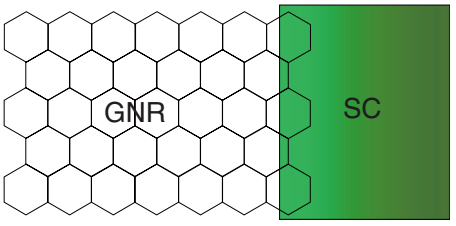

FIG. 1. (Color online) A hybrid junction between a zigzag graphene nanoribbon and a superconductor.

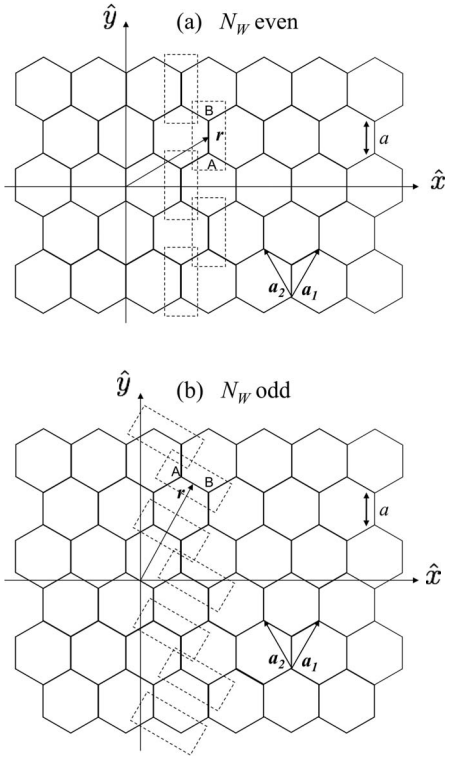

FIG. 2. Coordinates and elementary cells in GNRs in the cases where the number N_W of sites in the transverse direction is (a) even and (b) odd.

and provide analytical expressions for the GNR eigenfunctions, briefly discussing how transport properties of the hybrid GNR/SC junction are calculated. In Sec. III we report and discuss our results for the case of ideal GNRs, while in Sec. IV we discuss the role of nonideal edges. Finally, in Sec. V we summarize our main conclusions.

II. MODEL HAMILTONIAN, GNR EIGENFUNCTIONS, AND TRANSPORT PROPERTIES

We model the hybrid GNR/SC system by means of a tight-binding approach. In order to interpret the results presented below, we start by describing the eigenstates in the "normal" side of the junction (the GNR side). The GNR Hamiltonian $\mathcal{H}$ is a matrix with elements $\mathcal{H}_{ij}=-\gamma\delta_{\langle i,j\rangle}+U\delta_{ij}$, where γ is the hopping energy between nearest-neighbor sites $\langle \boldsymbol{i},\boldsymbol{j}\rangle$ on the honeycomb lattice and U accounts for a constant electrostatic energy, which can be controlled by a gate voltage.

Denoting by $\boldsymbol{a}_1$ and $\boldsymbol{a}_2$ as the honeycomb-lattice basis vectors, each unit cell is labeled by a vector $\boldsymbol{r}=n_1\boldsymbol{a}_1+n_2\boldsymbol{a}_2$, with n_1 and n_2 integers. The origin is located at the geometrical center of the GNR and N_W is the number of sites in the transverse direction $\hat{\boldsymbol{y}}$. A suitable shape of the cells turns out to depend on whether N_W is even or odd, as depicted in Fig. 2. One can show that the (unnormalized) eigenfunctions of a zigzag GNR at a cell $\boldsymbol{r}$ can be factorized in a longitudinal, a transverse, and a spin component. More explicitly,

$$\Psi_{p,\alpha}(x,y)=\Phi_p(x)\chi_p(y)w_\alpha, \tag{1}$$

where $p=A,B$ denotes the site type within the cell and $\alpha=\uparrow,\downarrow$ denotes the spin label. Here $x=a\sqrt{3}(n_1-n_2)/2$ and $y=3a(n_1+n_2)/2$ are the longitudinal and transverse coordinates of the cell vector $\boldsymbol{r}$, respectively ($a\simeq 1.42$ Å is the carbon-carbon distance). The longitudinal wave function in Eq. (1) reads

$$\Phi_p(x)=s_p(x)e^{ik_x x_p(x)}, \tag{2}$$

where k_x is the longitudinal wave vector and $x_p(x)$ is the coordinate of the p-type site belonging to the cell. Explicitly, $x_A=x_B=x$ if N_W is even, whereas $x_{A,B}=x\mp a\sqrt{3}/4$ if N_W is odd. The prefactor $s_p(x)=\pm 1$ in Eq. (2) is a sign,[24] and its presence stems from the fact that the ribbon bipartite lattice is invariant under longitudinal translations by an integer multiple of $\boldsymbol{a}_1-\boldsymbol{a}_2$ only. For energies $\lesssim\delta/4$ the transverse wave function reads[25]

$$\begin{pmatrix}\chi_A(y)\\ \chi_B(y)\end{pmatrix}=\begin{pmatrix}\sinh[k_y(W/2+y)]\\ \eta\sinh[k_y(W/2-y)]\end{pmatrix}, \tag{3}$$

where $W\equiv 3a\,\mathrm{int}[(N_W+1)/2]$ approximately coincides with the width of the GNR, with $\mathrm{int}[x]$ denoting the integer part of x. The transverse momentum k_y depends on the longitudinal momentum k_x. Details about such relation as well as the explicit expression for the eigenvalues will be discussed elsewhere.[26] Finally the spin-wave function w_α can be chosen as the $\hat{z}$-direction spinors $w_\uparrow=(1,0)^T$ and $w_\downarrow=(0,1)^T$. Importantly, beside momentum and spin, the eigenstates defined in Eqs. (1)–(3) exhibit an additional quantum number $\eta=\pm 1$, which determines whether the transverse cell wave function $(\chi_A+\chi_B)/2$ is even or odd with respect to the longitudinal axis of the GNR. One can therefore term η as pseudoparity. Note that in contrast to what happens in bulk graphene, states (1)–(3) are not eigenstates of the pseudospin-projection operator $\boldsymbol{\sigma}\cdot\hat{\boldsymbol{n}}$ for any unit vector $\hat{\boldsymbol{n}}$.

The eigenvalues ε obtained from the tight-binding equations as functions of k_x describe the band structure of the zigzag GNR, where two bands exhibit dispersionless zero modes (corresponding to states localized at the edges of the GNR) and the other ones are somewhat reminiscent of the bulk-graphene Dirac cones,[1] as illustrated in Fig. 3 for the case $U=0$. Energies are measured with respect to the Fermi level, and solid (dashed) lines refer to particles (holes) bands, which are degenerate for this particular case. The value of the pseudoparity η, shown inside the circles, alternates from a particle band to the next one and takes opposite values in particle and hole bands. Importantly, in the range $k_x a\sqrt{3}\in[0,\pi]$, the pseudoparity of a GNR with even N_W is opposite to the one for the case with odd N_W. This feature represents a hallmark of even/odd effect in pseudoparity, which cannot be seized by a continuum model description.

The energy separation δ between the first band and the zero-mode energy (Dirac level) is given by $\delta\simeq 9\pi\gamma/(6N_W-4)$ for even $N_W\gg 1$ or $\delta\simeq 3\pi\gamma/(2N_W-2)$ for odd $N_W\gg 1$.[27] Note that a finite U shifts the energy of the Dirac level away from the Fermi level, as shown in Fig. 4, breaking particle-hole degeneracy.[28]

The presence of the superconducting electrode is accounted for by the Bogoliubov–de Gennes Hamiltonian[29]

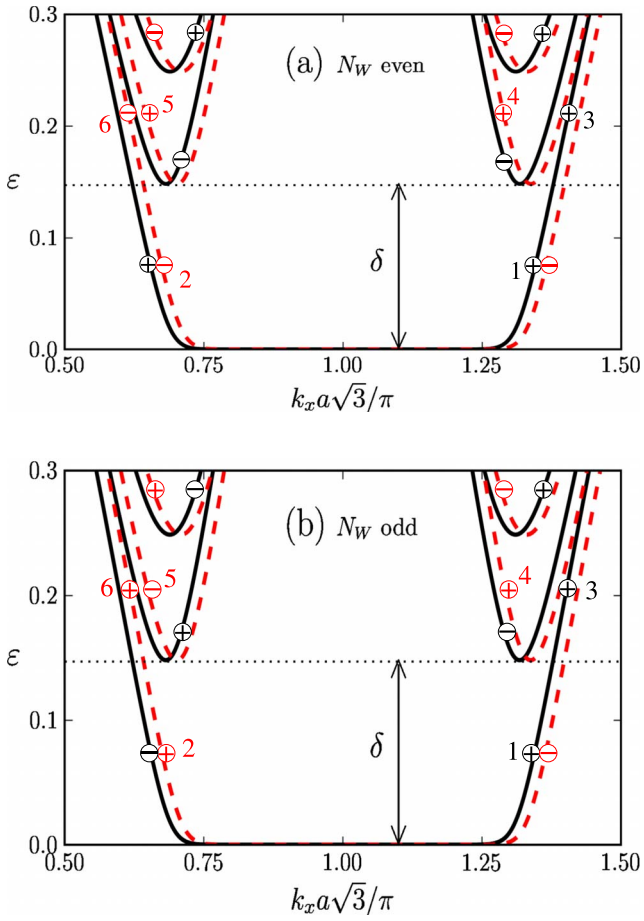

FIG. 3. (Color online) The band structure of a GNR as a function of the longitudinal wave vector k_x. Only the three lowest bands are illustrated. Energies are in units of γ. The solid (dashed) lines represent the particle (hole) bands. In this figure $U=0$ (zero gate voltage). In this case particle and hole bands are degenerate (for the sake of clarity the hole bands have been slightly shifted to the right). The signs + and − inside the circles indicate the value η of pseudoparity for each band. (a) N_W is even. In the range $0<\varepsilon<\delta$ no AR is possible since left-moving hole states 2 have pseudoparity opposite to the one of incoming right-moving particle states 1. In contrast, for $\varepsilon>\delta$, left-moving hole states 4 and 5 with the same pseudoparity as incoming particle states 3 are available, and AR is finite. (b) N_W is odd. In this case AR is possible in the range $0<\varepsilon<\delta$ since left-moving hole states 2 have the same pseudoparity of incoming right-moving particle states 1. For $\varepsilon>\delta$ left-moving hole states 4 and 6 with the same pseudoparity as incoming particle states 3 are available and AR is again possible. Note that left-moving hole state 5 in this case has pseudoparity opposite to the one of incoming right-moving particle states 3.

$$\mathcal{H}_{\mathrm{BdG}} = \begin{pmatrix} \mathcal{H} - \varepsilon_F & \Delta \\ \Delta^* & \varepsilon_F - \mathcal{H}^* \end{pmatrix}, \tag{4}$$

where $\mathcal{H}$ is the particle Hamiltonian and ε_F is the Fermi level of the GNR/SC junction at equilibrium. The SC (s-wave) order parameter, which couples particles and holes, is described by a matrix Δ with entries $\Delta_{ij}=\Delta_i\delta_{ij}$. Here Δ_i is taken to vary smoothly across the junction between its maximum value Δ_0 in the bulk of the SC and zero in the bulk of the GNR.[30]

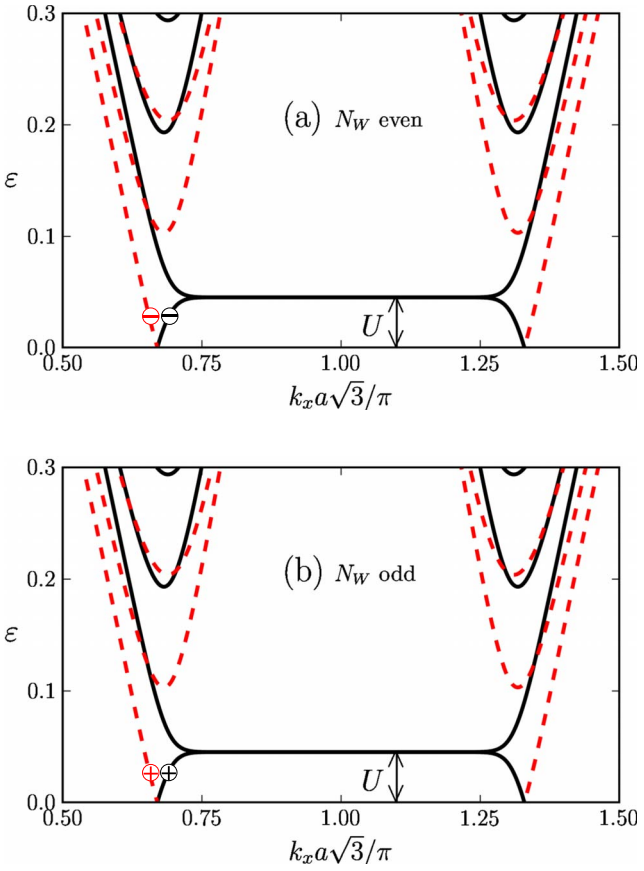

FIG. 4. (Color online) Same as in Fig. 3 but for $U\neq 0$ (finite gate voltage). In this case for $\varepsilon<U$ incoming particle states and outgoing hole states have the same pseudoparity, and AR is allowed.

Within the scattering approach[31] the zero-temperature differential conductance is given by[32,33]

$$G(V) \equiv \frac{dI}{dV} = \frac{2e^2}{h}[N(V) - R(V) + R_A(V)], \tag{5}$$

where V is the bias voltage applied across the junction. In Eq. (5) the prefactor 2 is due to spin degeneracy, whereas $N(V)$, $R(V)$, and $R_A(V)$ are the number of transverse propagating modes (open channels) available at energy eV measured from the Fermi level ε_F, the normal reflection coefficient, and the AR coefficient, respectively. Below the gap ($eV<\Delta_0$) only AR processes can contribute to the conductance since the unitarity of the scattering matrix implies that $N-R=R_A$ in this range.

III. RESULTS FOR THE IDEAL CASE

We present our numerical results, obtained using the numerical recursive Green's function technique, in the physically realistic regime $\delta \gg \Delta_0$. In this section we focus on the ideal case of a GNR with a fixed number of sites along the transverse direction. We first discuss the case where the

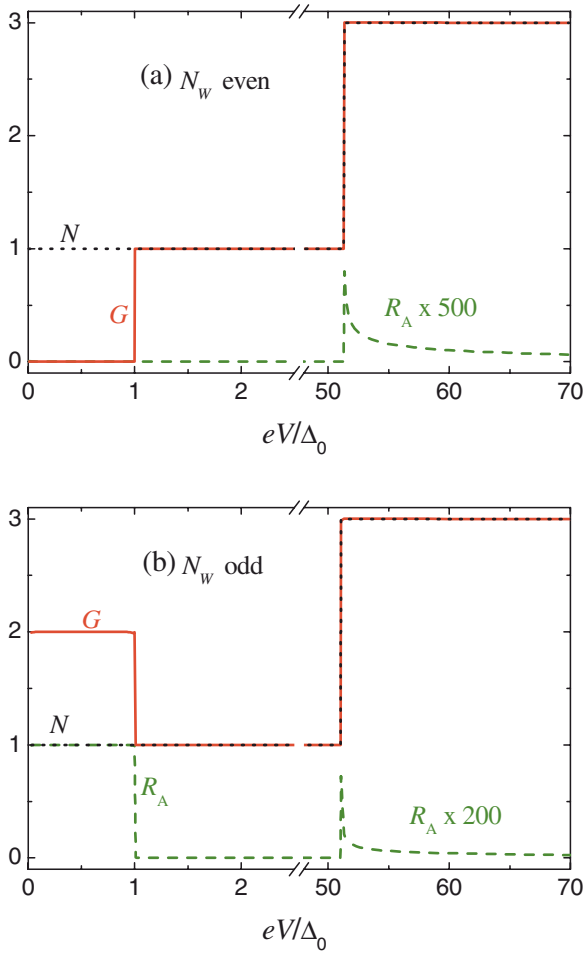

FIG. 5. (Color online) Transport properties of a GNR/SC interface. The differential conductance G in units of $2e^2/h$ (solid line), the total Andreev-reflection coefficient R_A (dashed line), and the number N of open channels (dotted line) are shown as functions of the applied bias eV (in units of Δ_0). Note that the horizontal axis has been broken in two ranges. The GNR has a width of about 50 nm, which corresponds to $\delta \sim 52$ meV$=52\Delta_0$ (the superconducting gap has been fixed at the value $\Delta_0=1$ meV and the hopping energy γ to the value 2.8 eV). (a) $N_W=250$. The AR coefficient is nonzero only for $eV>\delta$ and has been multiplied by a factor 500 for clarity. (b) $N_W=251$. The AR coefficient is unity for $eV<\Delta_0$, drops abruptly to zero for $eV>\Delta_0$, and remains zero up to $eV=\delta$. The AR coefficient is again finite for $eV>\delta$ and has been multiplied by a factor 200 for clarity.

Fermi level lies at the Dirac level ($U=0$) and then the case with a finite gate voltage $U\neq 0$.

A. Zero gate voltage

In Fig. 5(a) we plot G, R_A, and N as functions of the bias voltage applied across the junction for a GNR with even N_W, and in Fig. 5(b) we plot the same quantities for a GNR with odd N_W. In the subgap regime $eV<\Delta_0$ a striking dependence on the number of sites arises. While for even N_W the AR coefficient R_A *vanishes*, the opposite occurs for odd N_W, where R_A is unity. Because for $eV<\Delta_0$ electron transport is possible only by virtue of AR processes, the conductance G also vanishes in this voltage range for even N_W. In contrast, for odd N_W, G takes its maximum value in the same voltage range. In the regime $\Delta_0<eV<\delta$, where quasiparticle transmission becomes possible, R_A drops abruptly to zero also for odd N_W. This is due to the fact that the transmission processes, which are characterized by a small momentum transfer (intravalley), largely dominate over AR processes, which instead involve large momentum transfer (intervalley). We thus find a finite conductance with a value equal to the number N of open channels (in units of $2e^2/h$). Finally, for $eV>\delta$, R_A is finite but quite small in both cases (for clarity R_A has been multiplied by an enhancement factor) since voltages in this range are well above the superconducting gap.

These features ($R_A=0$ for $eV<\delta$ if N_W is even and $R_A=1$ for $eV<\Delta_0$ if N_W is odd) can be understood in terms of a pseudoparity superselection rule for the scattering states of the GNR. Let us consider a right-moving incoming electron (labeled by "1" in Fig. 2) with an energy lying between ε_F and the bottom of the second band. The only hole state available for an AR process is the one labeled by "2", which is characterized by a pseudoparity η that is (i) *opposite* to the one of the incoming electron for even N_W and (ii) *equal* to the one of the incoming electron for odd N_W.

A superconducting parameter that is constant along the transverse direction cannot couple states with opposite pseudoparity (i.e., the pseudoparity of an electron impinging onto the SC interface cannot be flipped). Thus for even N_W the AR process is forbidden and R_A vanishes, whereas for odd N_W this process is allowed and R_A is finite. Notice that in the latter case normal reflection is forbidden by pseudoparity conservation, yielding $R_A=1$ in the subgap regime. For $\Delta_0<eV<\delta$ normal transmission is the dominating process, so that R_A is strongly suppressed for both even and odd N_W. A finite AR is restored for $eV>\delta$. Indeed in this case intravalley scattering into hole states with the appropriate pseudoparity ["4" in Figs. 3(a) and 3(b)] is available. This superselection rule is the ribbon counterpart of the bulk Klein-paradox selection rules based on pseudospin[2] and also explains the valley-valve effect in p-n junctions in GNRs.[21–23]

B. Finite gate voltage

Let us now consider the case $U\neq 0$ (and $U\ll\delta$). In Fig. 6 we plot our results for G, R_A, and N.

A comparison between Figs. 5(a) and 6(a) shows that the application of a gate voltage has dramatic consequences on electron conduction in GNRs with even N_W. This is evident from Fig. 4(a). AR processes are allowed by pseudoparity conservation in the bias range $eV<U$, while they are forbidden for $U<eV<\delta$. This fact is reflected in the results shown in Fig. 6(a), where the differential conductance is finite (and equal to $4e^2/h$) for $eV<U$ and vanishes in the range[34] $U<eV<\sqrt{U^2+\Delta_0^2}$. For subgap voltages electron conduction can be switched on and off by the application of a gate voltage. The junction between an even-N_W GNR and a SC exhibits the operational behavior of an electron transistor based on the pseudoparity conservation law.

In contrast, for odd N_W the application of a gate voltage is expected to have no major qualitative impact on the transport

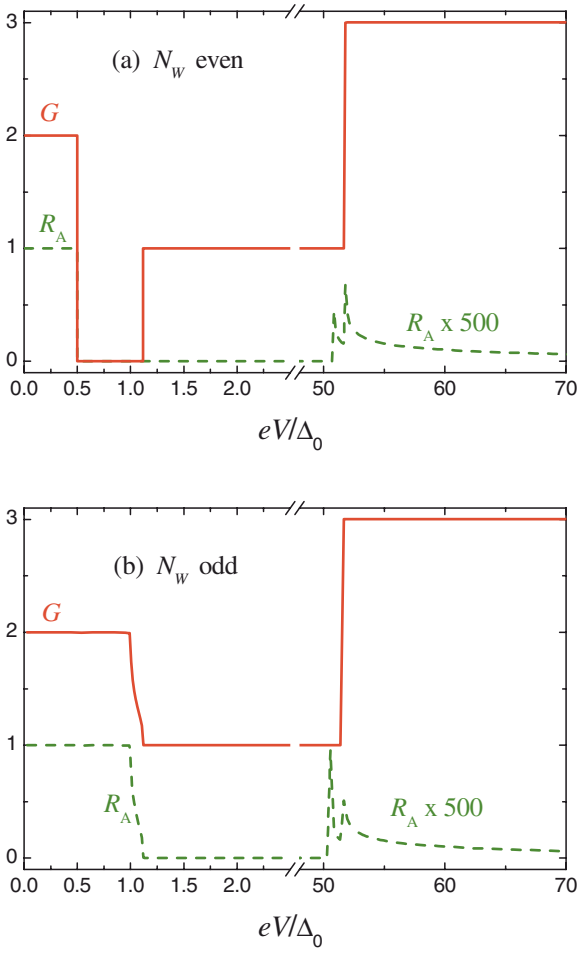

FIG. 6. (Color online) Same as in Fig. 5 but for $U=0.5\Delta_0$ (in this figure we have not plotted the number of open channels). (a) N_W is even. In this case the AR coefficient is restored to a finite value for $eV<U$, while it remains zero for $U<eV<\delta$. (b) N_W is odd. In this case no big qualitative changes are seen to occur by switching on a finite value of U.

properties of a junction between a GNR with odd N_W and a SC. Once again, this expectation can be traced back to the pseudoparity quantum number, as depicted in Fig. 4(b). The data reported in Fig. 6(b) show indeed the same qualitative behavior reported in Fig. 5(b). The only slight modification is that the drop of R_A to zero, in the range $eV \gtrsim \Delta_0$, is less abrupt than in Fig. 5(b) due to a slight momentum mismatch in the transmission channel between GNR and SC sides, arising when $U \neq 0$.

Before concluding we would like to comment on the double-spike structure of R_A at voltages $eV=\delta \pm U$, which is seen in both panels of Fig. 6. This is due to the opening of additional channels for AR processes made available by the existence of the first-excited energy band (see Fig. 4).

IV. RESULTS FOR THE NONIDEAL CASE

In experimental realizations of GNRs the number of transverse sites varies along the longitudinal direction. Here we present a study of these "nonideal" effects on the predictions

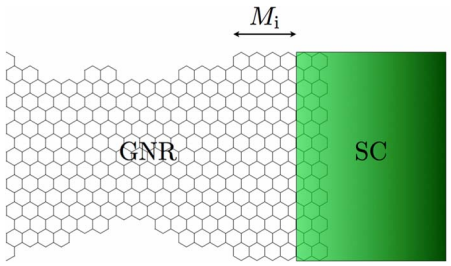

FIG. 7. (Color online) Schematic representation of a GNR with nonideal edges.

made in Sec. III. For the sake of generality, we focus our attention on the case $U \neq 0$.

We introduce a more realistic model for a GNR by altering the upper and the lower edge profiles with respect to the ideal case depicted in Fig. 1. A typical nonideal edge configuration we have considered is depicted in Fig. 7. The number of sites in the transverse direction is changed by one unit in a stepwise fashion, independently along each edge (see Fig. 7). The average step length is taken to be equal to $\bar{M}$ in both edges. The strip close to the interface with the SC has a length $M_i=\bar{M}$ and a width $N_{W,i}$. In what follows we will show that what really determines the behavior of the junction is the parity of this strip, provided that M_i is sufficiently large.

In Fig. 8 we present numerical results for the nonlinear conductance for three values of $\bar{M}$ ($\bar{M}=4$, 6, and 8) and for a maximum width variation in four sites. Also in this case we present separately the results for even and odd $N_{W,i}$. In Fig. 8(a) ($N_{W,i}$ is even) we observe that the sharp drop of R_A and G at $eV=U$ that we had in the ideal case [see Fig. 6(a)] has changed into a smooth crossover over a bias interval δV. We find that δV decreases with increasing $\bar{M}$; for $\bar{M}=8$ the conductance behavior is essentially identical to the ideal one. A similar behavior is observed for odd $N_{W,i}$; see Fig. 8(b). Note that for small $\bar{M}$ sharp antiresonances occur at energies $eV \simeq U$.

Because δV decreases with increasing $\bar{M}$, below we determine the minimum value of $\bar{M}$, $M^\star$, which leads to a substantially ideal behavior. To do so, we analyze a simplified case in which the GNR is made up of two regions. The strip of length M_i is connected to a region with a number of transverse sites that differs by one unit from $N_{W,i}$. The junction is said to be ideal if its AR coefficient satisfies the following inequality: $|R_A(V)-R_A^{\text{ideal}}(V)|<10^{-2}$ for every V such that $|eV-U|/\Delta_0>10^{-2}$.

In Fig. 9 we report $M^\star$ as a function of $N_{W,i}$ (even case). Two comments are in order at this point: (i) since $M^\star \ll N_{W,i}$, a relatively narrow strip close to the SC is sufficient to ensure the ideal behavior of the junction described in Sec. III and (ii) $M^\star$ decreases with increasing $N_{W,i}$, saturating when $N_{W,i} \simeq 150$. The asymptotic value to which $M^\star$ saturates (in the case of Fig. 9 it is roughly eight) depends on the specific criterion that one chooses. A similar scenario applies to the case of odd $N_{W,i}$. This curve supports the numerical results illustrated in Fig. 8; for a GNR with $N_{W,i}=100$ the

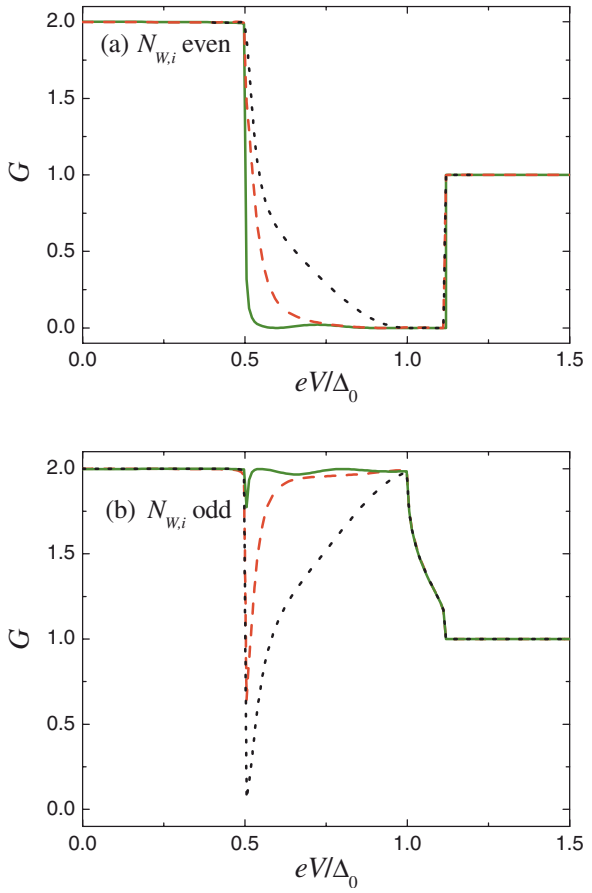

FIG. 8. (Color online) The differential conductance G in units of $2e^2/h$ is shown as a function of the applied bias eV (in units of Δ_0) for various values of $\bar{M}$. (a) $N_{W,i}=100$. The (black) short-dashed line corresponds to $\bar{M}=4$, whereas the (red) long-dashed line and the (green) solid line correspond to $\bar{M}=6$ and $\bar{M}=8$, respectively. (b) Same as in panel (a) but for $N_{W,i}=101$. For $\bar{M}=8$ the ideal-GNR behavior depicted in Fig. 6 is almost recovered.

threshold length is roughly ten, explaining why the results corresponding to $\bar{M}=4$ depart substantially from ideality.

V. CONCLUSIONS

In summary, we have studied Andreev reflection in graphene nanoribbon/superconductor hybrid junctions. We have reported analytical expressions for the eigenfunctions of the tight-binding Hamiltonian describing the graphene nanoribbon, which carry explicitly a definite pseudoparity. The superselection rule stemming from this quantum number has two main implications on transport through the hybrid junction. For narrow nanoribbons with an even number of sites in the transverse direction, we have found a complete suppression of Andreev reflection in a range of energies that is huge

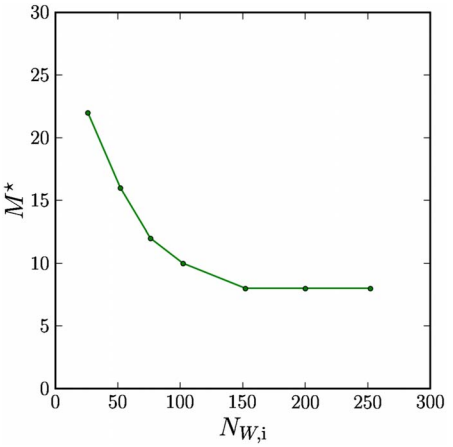

FIG. 9. (Color online) The threshold length $M^\star$ as a function of $N_{W,i}$ (even case only).

when the Fermi energy lies at the Dirac level. This implies zero conductance at subgap voltages, which can however be restored by applying a finite gate potential, opening up potential technological applications of these hybrid junctions as electron transistors as well as nanorefrigerators. In contrast, in the case of narrow nanoribbons with an odd number of sites, we have found perfect Andreev reflection at subgap voltages and an abrupt suppression of it at supergap voltages.

We have also examined the case of nonideal nanoribbons in which the number of transverse sites varies along the transport direction. We have found that the transport properties of the junction in this case are determined by the parity of the region close to the interface with the superconductor. The behavior of the junction is indeed essentially ideal, provided that its length is larger than a certain threshold. These findings are relevant to realistic hybrid junctions between a graphene flake and a superconductor. Even for micrometer-sized flakes finite-size effects play a very important role since the confinement-induced mean energy spacing is larger than the superconducting gap.

The role of electron-electron interactions and/or next-nearest-neighbor hopping, which has not been addressed in the present work, can be qualitatively understood along the following lines. These effects have been shown to lead to the opening of a gap Δ_g at the Dirac level,[1,16] which is however typically much smaller than δ. Our conclusions thus remain valid for a large range of energies even when these effects are taken into account.

ACKNOWLEDGMENTS

We gratefully acknowledge C. Beenakker and F. Guinea for very useful discussions and suggestions. This work was partly supported by the NANOFRIDGE EU Project and by the CNR-INFM "Seed Projects." F.D. also acknowledges the financial support of "Programma Rientro Cervelli" by the Italian MIUR.

*d.rainis@sns.it

[1] A. K. Geim and K. S. Novoselov, Nature Mater. **6**, 183 (2007); A. K. Geim and A. H. MacDonald, Phys. Today **60** (8), 35 (2007); A. H. Castro Neto, F. Guinea, N. M. R. Peres, K. S. Novoselov, and A. K. Geim, Rev. Mod. Phys. **81**, 109 (2009).

[2] M. I. Katsnelson, K. S. Novoselov, and A. K. Geim, Nat. Phys. **2**, 620 (2006).

[3] C. W. J. Beenakker, Phys. Rev. Lett. **97**, 067007 (2006); M. Titov and C. W. J. Beenakker, Phys. Rev. B **74**, 041401(R) (2006); C. W. J. Beenakker, Rev. Mod. Phys. **80**, 1337 (2008).

[4] T. Ludwig, Phys. Rev. B **75**, 195322 (2007).

[5] J. Linder and A. Sudbo, Phys. Rev. Lett. **99**, 147001 (2007); Phys. Rev. B **77**, 064507 (2008).

[6] J. C. Cuevas and A. L. Yeyati, Phys. Rev. B **74**, 180501(R) (2006).

[7] J. Cayssol, Phys. Rev. Lett. **100**, 147001 (2008).

[8] E. Prada, P. San-Jose, B. Wunsch, and F. Guinea, Phys. Rev. B **75**, 113407 (2007).

[9] See, for example, S. Bhattacharjee and K. Sengupta, Phys. Rev. Lett. **97**, 217001 (2006); A. G. Moghaddam and M. Zareyan, Phys. Rev. B **74**, 241403(R) (2006); M. Titov, A. Ossipov, and C. W. J. Beenakker, *ibid.* **75**, 045417 (2007); A. R. Akhmerov and C. W. J. Beenakker, *ibid.* **75**, 045426 (2007); A. Ossipov, M. Titov, and C. W. J. Beenakker, *ibid.* **75**, 241401(R) (2007); D. Greenbaum, S. Das, G. Schwiete, and P. G. Silvestrov, *ibid.* **75**, 195437 (2007); M. Maiti and K. Sengupta, *ibid.* **76**, 054513 (2007); J. Gonzalez and E. Perfetto, *ibid.* **76**, 155404 (2007); S. Bhattacharjee, M. Maiti, and K. Sengupta, *ibid.* **76**, 184514 (2007); G. Tkachov, *ibid.* **76**, 235409 (2007); K. Sasaki *et al.*, J. Phys. Soc. Jpn. **76**, 033702 (2007); B. Uchoa and A. H. Castro Neto, Phys. Rev. Lett. **98**, 146801 (2007); A. R. Akhmerov and C. W. J. Beenakker, *ibid.* **98**, 157003 (2007); C. W. J. Beenakker, A. R. Akhmerov, P. Recher, and J. Tworzydło, Phys. Rev. B **77**, 075409 (2008); T. Yokoyama, J. Linder, and A. Sudbo, *ibid.* **77**, 132503 (2008); P. Burset, A. L. Yeyati, and A. Martin-Rodero, *ibid.* **77**, 205425 (2008); J. Linder, T. Yokoyama, D. Huertas-Hernando, and A. Sudbø, Phys. Rev. Lett. **100**, 187004 (2008); C. Benjamin and J. K. Pachos, Phys. Rev. B **78**, 235403 (2008); A. M. Black-Schaffer and S. Doniach, Phys. Rev. B **78**, 024504 (2008); M. Zareyan, H. Mohammadpour, and A. G. Moghaddam, Phys. Rev. B **78**, 193406 (2008), and other related works cited in these papers.

[10] A. F. Andreev, Sov. Phys. JETP **19**, 1228 (1964).

[11] A. Shailos, W. Nativel, A. Kasumov, C. Collet, M. Ferrier, S. Gueron, R. Deblock, and H. Bouchiat, Europhys. Lett. **79**, 57008 (2007).

[12] F. Miao, S. Wijeratne, U. Coskun, Y. Zhang, and C. N. Lau, arXiv:cond-mat/0703052 (unpublished).

[13] H. B. Heersche, P. Jarillo-Herrero, J. B. Oostinga, L. M. K. Vandersypen, and A. F. Morpurgo, Nature (London) **446**, 56 (2007).

[14] X. Du, I. Skachko, and E. Y. Andrei, Phys. Rev. B **77**, 184507 (2008).

[15] Z. Chen, Y.-M. Lin, M. J. Rooks, and P. Avouris, Physica E **40**, 228 (2007); M. Y. Han, B. Özyilmaz, Y. Zhang, and P. Kim, Phys. Rev. Lett. **98**, 206805 (2007); X. Li, X. Wang, L. Zhang, S. Lee, and H. Dai, Science **319**, 1229 (2008); X. Wang, Y. Ouyang, X. Li, H. Wang, J. Guo, and H. Dai, Phys. Rev. Lett. **100**, 206803 (2008); Y.-M. Lin, V. Perebeinos, Z. Chen, and P. Avouris, Phys. Rev. B **78**, 161409(R) (2008).

[16] See, e.g., Y.-W. Son, M. L. Cohen, and S. G. Louie, Phys. Rev. Lett. **97**, 216803 (2006); V. Barone, O. Hod, and G. E. Scuseria, Nano Lett. **6**, 2748 (2006); L. Yang, C.-H. Park, Y.-W. Son, M. L. Cohen, and S. G. Louie, Phys. Rev. Lett. **99**, 186801 (2007).

[17] L. Brey and H. A. Fertig, Phys. Rev. B **75**, 125434 (2007).

[18] L. Malysheva and A. Onipko, Phys. Rev. Lett. **100**, 186806 (2008); A. Onipko, Phys. Rev. B **78**, 245412 (2008).

[19] M. I. Katsnelson and F. Guinea, Phys. Rev. B **78**, 075417 (2008).

[20] A. R. Akhmerov and C. W. J. Beenakker, Phys. Rev. B **77**, 085423 (2008).

[21] K. Wakabayashi and T. Aoki, Int. J. Mod. Phys. B **16**, 4897 (2002).

[22] A. R. Akhmerov, J. H. Bardarson, A. Rycerz, and C. W. J. Beenakker, Phys. Rev. B **77**, 205416 (2008).

[23] A. Cresti, G. Grosso, and G. P. Parravicini, Phys. Rev. B **77**, 233402 (2008).

[24] If one chooses $k_x \in [-\pi/(a\sqrt{3}), \pi/(a\sqrt{3})]$ then $s_p(x)=(-1)^{n_1-n_2}$ for even N_W, whereas $s_A=(-1)^{n_1-n_2}$ and $s_B=(-1)^{n_1-n_2+1}$ for odd N_W.

[25] At higher energies and for the other bands the evanescent waves (3) become less localized at the edges (Ref. 28) and eventually turn into an oscillatory behavior when k_y becomes imaginary. Nevertheless, the characterization of the bands via the pseudoparity quantum number holds at all energies, as depicted in Fig. 3.

[26] D. Rainis *et al.* (unpublished).

[27] A. Rycerz, J. Tworzydlo, and C. W. J. Beenakker, Nat. Phys. **3**, 172 (2007).

[28] See, e.g., A. Rycerz and C. W. J. Beenakker, arXiv:0709.3397 (unpublished); A. Rycerz, Phys. Status Solidi A **205**, 1281 (2008).

[29] P. G. de Gennes, *Superconductivity of Metals and Alloys* (Addison-Wesley, New York, 1989).

[30] Notice that since graphene honeycomb lattice is bipartite, a simplified model in which Δ_i is assumed as a steplike function along the $\hat{x}$ direction would effectively imply a rapid variation in Δ_i also transversally along the two-site cells. Since such situation would not be realistic, we have adopted a smooth variation in Δ_i over a length $\lambda \simeq 10a$ along the $\hat{x}$ direction.

[31] S. Datta, *Electronic Transport in Mesoscopic Systems*(Cambridge University Press, Cambridge, 1995).

[32] G. E. Blonder, M. Tinkham, and T. M. Klapwijk, Phys. Rev. B **25**, 4515 (1982); C. J. Lambert, J. Phys.: Condens. Matter **3**, 6579 (1991); C. J. Lambert and R. Raimondi, *ibid.* **10**, 901 (1998).

[33] C. J. Lambert, V. C. Hui, and S. J. Robinson, J. Phys.: Condens. Matter **5**, 4187 (1993).

[34] The fact that G vanishes in the range $\Delta_0 < eV < \sqrt{U^2+\Delta_0^2}$ can also be understood in terms of pseudoparity conservation.